Structure

Cholesterol occupies the lipid translocation pathway to block phospholipid scrambling by a G protein-coupled receptor

Graphical abstract

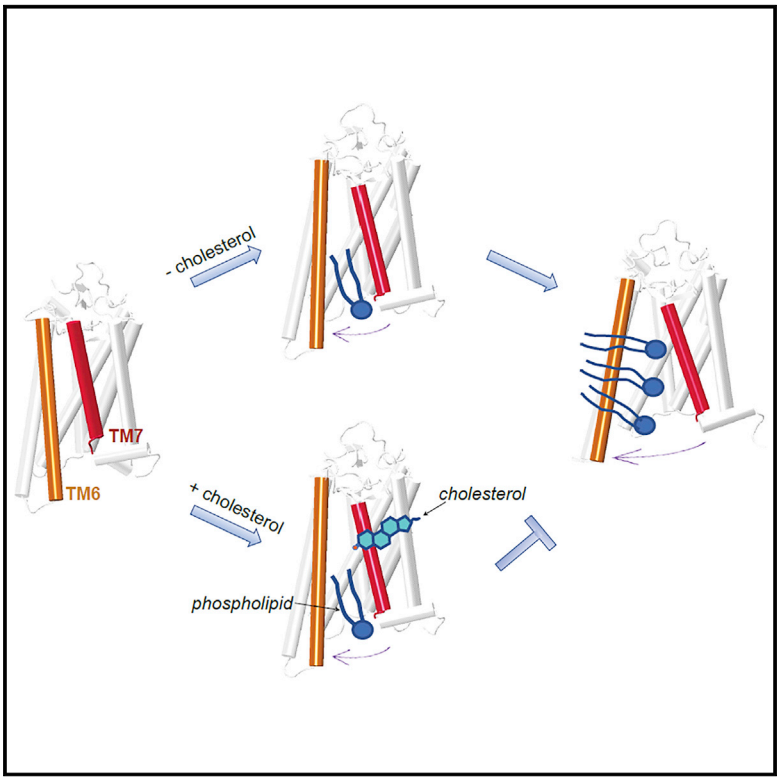

Authors

Giulia Morra, Asghar M. Razavi, Anant K. Menon, George Khelashvili

Correspondence

gek2009@med.cornell.edu

In brief

Morra et al. present comparative analyses of molecular dynamics simulations of the G protein-coupled receptor opsin in cholesterol-free and cholesterol-rich membranes. Their results provide insights into the molecular mechanism by which cholesterol inhibits GPCR-mediated phospholipid scrambling and explain the apparent inability of GPCRs to scramble lipids at the plasma membrane.

Highlights

- Effect of membrane cholesterol on opsin-mediated phospholipid scrambling
- Large-scale molecular dynamics simulations of opsin in a cholesterol-rich membrane
- Cholesterol stabilizes the closed state of the phospholipid translocation pathway
- Closed pathway prevents phospholipid scrambling, while allowing cholesterol flip-flop

Morra et al., 2022, Structure *30*, 1208–1217
August 4, 2022
https://doi.org/10.1016/j.str.2022.05.010

CellPress

CellPress

Structure

Theory

Cholesterol occupies the lipid translocation pathway to block phospholipid scrambling by a G protein-coupled receptor

Giulia Morra,[1,2,6] Asghar M. Razavi,[3,6] Anant K. Menon,[4] and George Khelashvili[1,5,7,*]

[1]Department of Physiology and Biophysics, Weill Cornell Medicine, 1300 York Avenue, Room LC-501C, New York, NY 10065, USA
[2]Istituto di Scienze e Tecnologie Chimiche SCITEC, CNR, Via Mario Bianco 9, 20131 Milano, Italy
[3]Roivant Sciences, New York, NY 10036, USA
[4]Department of Biochemistry, Weill Cornell Medicine, New York, NY 10065, USA
[5]Institute for Computational Biomedicine, Weill Cornell Medicine, New York, NY 10065, USA
[6]These authors contributed equally
[7]Lead contact
*Correspondence: gek2009@med.cornell.edu
https://doi.org/10.1016/j.str.2022.05.010

SUMMARY

Class A (rhodopsin-like) G protein-coupled receptors (GPCRs) are constitutive phospholipid scramblases as evinced after their reconstitution into liposomes. Yet phospholipid scrambling is not detectable in the resting plasma membrane of mammalian cells that is replete with GPCRs. We considered whether cholesterol, a prominent component of the plasma membrane, limits the ability of GPCRs to scramble lipids. Our previous Markov State Model (MSM) analysis of molecular dynamics simulations of membrane-embedded opsin indicated that phospholipid headgroups traverse a dynamically revealed hydrophilic groove between transmembrane helices (TM) 6 and 7 while their tails remain in the bilayer. Here, we present comparative MSM analyses of 150-μs simulations of opsin in cholesterol-free and cholesterol-rich membranes. Our analyses reveal that cholesterol inhibits phospholipid scrambling by occupying the TM6/7 interface and stabilizing the closed groove conformation while itself undergoing flip-flop. This mechanism may explain the inability of GPCRs to scramble lipids at the plasma membrane.

INTRODUCTION

Class A G protein-coupled receptors (GPCRs), such as the visual pigment rhodopsin, the β1-and β2-adrenergic receptors, and the adenosine A2A receptor, have been shown to moonlight as constitutive phospholipid scramblases (Ernst and Menon, 2015; Goren et al., 2014; Khelashvili and Menon, 2021; Menon et al., 2011). On reconstitution into large unilamellar vesicles, these proteins scramble phospholipids at a rate $>10^4$ s^{-1}, several orders of magnitude faster than the rate of spontaneous lipid flip-flop ($\sim10^{-5}$ s^{-1}) (Pomorski and Menon, 2006). The scramblase activity of rhodopsin has been suggested to be important for the homeostasis of photoreceptor disc membranes by providing a mechanism to repair the trans-bilayer phospholipid imbalance caused by the unidirectional lipid pumping activity of disc-localized ATP-driven transporters, including the ABCA4 transporter whose functional deficiency is associated with Stargardt disease (Ernst and Menon, 2015; Molday et al., 2021; Quazi et al., 2012; Quazi and Molday, 2014). More generally, it has been proposed that GPCRs may contribute to phospholipid scramblase activity in the secretory pathway (Ernst and Menon, 2015; Goren et al., 2014), especially in the endoplasmic reticulum where phospholipids are synthesized on the cytoplasmic face (Chauhan et al., 2016) and must be scrambled to populate the luminal leaflet for membrane growth.

The mechanism by which opsin and other GPCRs facilitate lipid scrambling has not been experimentally elucidated, but our computational studies of opsin in a lipid membrane (Morra et al., 2018) suggest a molecular mechanism of rapid lipid translocation that is consistent with the "credit card" model (Pomorski and Menon, 2006) (Figure 1A). Thus, Markov State Model (MSM) analysis of large-scale atomistic molecular dynamics (MD) simulations of opsin in 9:1 POPC (1-palmitoyl-2-oleoyl-*sn*-glycero-3-phosphocholine)/POPG (1-palmitoyl-2-oleoyl-*sn*-glycero-3-phospho-(1′-rac-glycerol)) lipid membrane (Morra et al., 2018) revealed a pathway for lipid translocation along the interface between transmembrane helices (TMs) 6 and 7 of the protein (Figure 1B). This pathway was enabled by local conformational changes at two regions along the TM6/7 interface (see Stage 1 snapshot in Figure 1B): at the intracellular ends of TM6 and TM7 (S1 site), interactions between residues $E249^{6.32}$ on TM6 and $K311^{7.53}$ on TM7 were broken, leading to a widening and hydration of this part of the interface (throughout the text, superscripts refer to the Ballesteros-Weinstein generic numbering of residues in GPCR proteins [Ballesteros and Weinstein, 1995]). This was followed by disruption of interactions

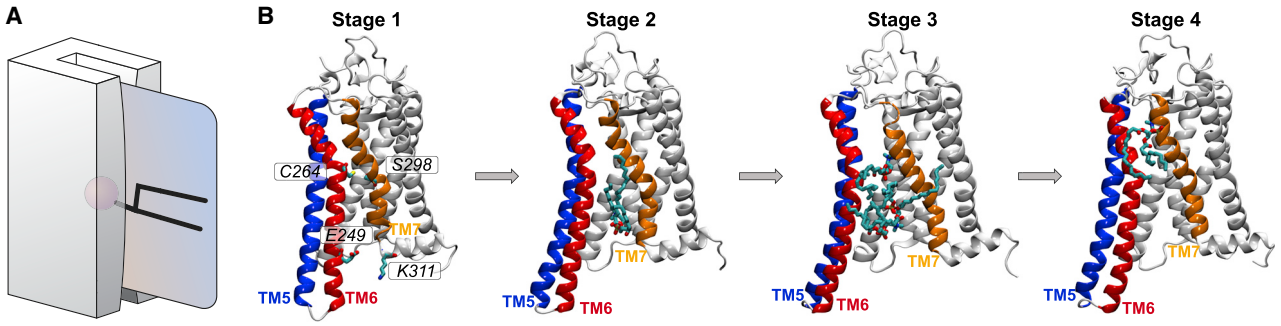

Figure 1. Lipids traverse the hydrophilic pathway in opsin according to the credit card mechanism

(A) Credit card model of *trans*-bilayer lipid movement through opsin (modified from Pomorski and Menon, 2006).

(B) Snapshots illustrating the gradual opening of the lipid pathway in the adaptive ensemble molecular dynamics simulations reported in Morra et al. (Morra et al., 2018). Through stages 1–4 of the simulations, the hydrophilic translocation pathway is dynamically revealed between TMs 6 and 7. In the snapshots, TMs 5, 6, and 7 are colored in blue, red, and orange, respectively. The penetrating lipids are shown in stick representation. Residue pairs E249$^{6.32}$-K311$^{7.58}$ and C264$^{6.47}$-S298$^{7.45}$ demarcating the locations of two key sites along the translocation pathway, S1 and S2, are illustrated in the Stage 1 snapshot.

between C264$^{6.47}$ (TM6) and S298$^{7.45}$ (TM7) in the middle part of the interface (S2 site). Together these dynamic events repositioned TMs 6 and 7 away from each other and transformed the region into a continuous aqueous conduit that was exploited by lipid headgroups to translocate between the two leaflets while the hydrophobic tails of the scrambled lipids remained in the bilayer environment (reviewed in Ref. Khelashvili and Menon, 2021).

Whereas these computational studies provided important mechanistic insights into GPCR-mediated lipid scrambling, we were curious to learn whether and how the scrambling process might be affected by the membrane lipid environment. The significance of this issue is evident when considering the plasma membrane of mammalian cells, which is replete with class A GPCRs (HEK293T cells express at least 75 different GPCRs amounting to approximately 10^5 receptors per cell [Khelashvili and Menon, 2021]), yet it remains strongly asymmetric, with no evidence of constitutive lipid scrambling activity (Kobayashi and Menon, 2018). The specialized plasma membrane of photoreceptor outer segments (Albert et al., 2016; Albert and Boesze-Battaglia, 2005) also lacks constitutive scramblase activity (Ruggiero et al., 2012) even though it contains rhodopsin (Molday and Molday, 1987). This raises the possibility that GPCR scramblases may be silenced by the unique physical characteristics of the plasma membrane, for example high cholesterol content and prevalence of lipids with saturated acyl chains (Holthuis and Menon, 2014).

Cholesterol is a strong driver of membrane physical properties (Regen, 2022) and is also known to bind GPCRs (Pucadyil and Chattopadhyay, 2006; Taghon et al., 2021). As such, it may affect conformational dynamics of GPCRs needed to reveal the TM6-TM7 lipid pathway and therefore influence scrambling mechanisms. Of note, rhodopsin molecules located in the cholesterol-rich plasma membrane of photoreceptor outer segments are unable to execute the light-induced conformational changes necessary for signaling but become competent to do so when cholesterol is eliminated (Boesze-Battaglia and Albert, 1990), implicating cholesterol in receptor function.

Here, using a combination of MSMs and ensemble MD simulations of opsin, we probed the effects of cholesterol on the scrambling mechanism. We extended the timescales of the earlier MD simulations of opsin in 9:1 POPC/POPG membranes by collecting a much larger trajectory set (cumulative sampling time of 150 μs) to allow rigorous sampling of rare dynamic events during the scrambling process and generate a new set of comparably long ensemble MD trajectories of opsin in cholesterol-enriched membranes (60:30:10 POPC/cholesterol/POPG). Comparative analysis of the two trajectory sets revealed specific modes of cholesterol arrangement at the S2 site, in the central part of the TM6/7 interface (Figure 1), which stabilized the closed conformation of the translocation pathway and thus inhibited lipid scrambling. Remarkably, we found that the closed pathway was permissive to cholesterol flip-flop as the sterol was seen to transit between the leaflets through the S2 site, with its small polar hydroxyl group engaging with the membrane exposed T297$^{7.44}$/S298$^{7.45}$ pair of residues on TM7. Together, our results suggest that cholesterol molecules compete with phospholipids for the S2 site as they diffuse between the leaflets. We propose that this competition mechanism may inhibit opsin-mediated lipid scrambling.

RESULTS

Generation of comparative sets of unbiased MD simulations of opsin in cholesterol-free and cholesterol-rich membranes

We previously reported on conformational dynamics in opsin that resulted in opening of a hydrophilic pathway between TMs 6 and 7 that was traversed by lipids, enabling scrambling by the credit card reader mechanism (Figure 1) (Morra et al., 2018). These insights were inferred from ensemble atomistic MD simulations of opsin in phospholipid membranes (9:1 POPC/POPG mol/mol) that were carried out according to a multi-stage adaptive protocol, whereby each stage was informed by the output from the previous stage. While revealing detailed mechanistic insights about GPCR-mediated lipid scrambling, these computational experiments, due to their adaptive nature, did not adequately sample rare dynamic events during the scrambling process. Therefore, this simulation set could not be used for quantitative comparison of scrambling

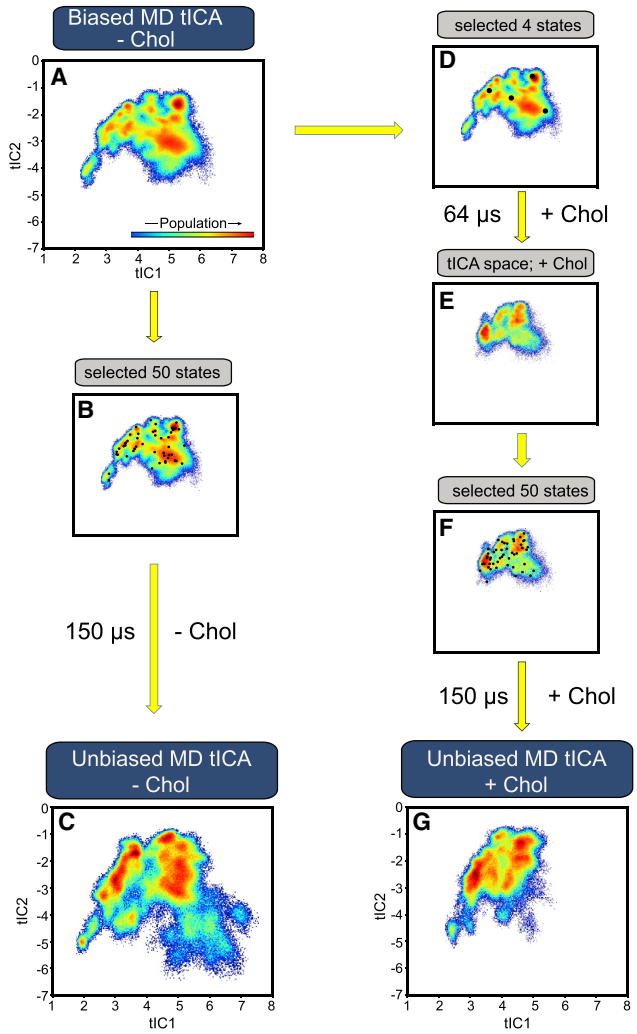

Figure 2. Generation of unbiased MD simulations for opsin in POPC/POPG (–Chol) and POPC/POPG/cholesterol (+30 mole % Chol) membrane

(A) Dimensionally reduced representation of the MD simulations from Morra et al. (2018) obtained by projecting the trajectory frames along the first two slowest components of tICA transformation.

(B) Discretization of the 2D space from (A) into 50 microstates.

(C) The tICA landscape of 150-µs ensemble MD simulations of –Chol system initiated from the microstate centroid structures in (B).

(D) The tICA space from (A) showing location of the four conformations (illustrated in Figure 1) used to initiate simulations of opsin in +Chol membrane.

(E) The tICA landscape of 64-µs ensemble MD simulations in +Chol membrane.

(F) Discretization of the 2D space from (E) into 50 microstates.

(G) The tICA landscape of 150-µs ensemble MD simulations of +Chol system initiated from the microstate centroid structures in (F).

mechanisms under different conditions, such as in the presence or absence of cholesterol.

To address this deficiency, we carried out a new and much larger set of unbiased MD simulations of opsin GPCR in cholesterol-free and cholesterol-rich membranes. The simulations in cholesterol-free membranes captured four full lipid scrambling events (i.e., the translocation pathway was fully traversed by lipids) and five incomplete scrambling events (the translocation pathway was partially traversed by lipids). The simulations in cholesterol-rich membranes captured a single event of full lipid scrambling, a single event of partial lipid scrambling, and five events of full cholesterol scrambling (see below).

Starting configurations for these runs were based on the conformational sampling achieved in the older trajectory set (described in Morra et al., 2018 and referred to throughout as the biased MD set). More specifically, Figure 2A shows a dimensionally reduced representation of the MD simulations from Morra et al. (2018) obtained by projecting the trajectory frames along the first two slowest components of tICA (time-lagged independent component analysis) transformation (tIC1 and tIC2 vectors, see STAR Methods). To generate starting conformations for a new set of unbiased simulations for opsin in cholesterol-depleted membranes, the 2D tICA space was clustered into 50 microstates (Figure 2B), and the centroid structures from each microstate were subjected to 3-µs-long unbiased MD simulations, resulting in 150-µs trajectory sampling. The tICA landscape corresponding to this simulation set is depicted in Figure 2C.

To produce a similarly extensive unbiased sampling of opsin dynamics in a cholesterol-rich membrane, we chose four conformations of the protein from the biased MD set (Figure 2D), differing in the extent of the opening of the lipid scrambling pathway (Figure 1), and we embedded these structures in the cholesterol-containing lipid bilayer. The resulting four systems were simulated in 20 independent replicates, each 800 ns (cumulative 64 µs MD). The trajectories were then projected onto the same tICA space (Figure 2E), and the resulting landscape was discretized into 50 microstates (Figure 2F). The conformations representing centroids of each microstate were then used to initiate 3-µs-long ensemble MD simulations. The projection of these trajectories onto the tICA space is presented in Figure 2G. Thus, for both, cholesterol-free and cholesterol-rich systems, we accumulated 150 µs of unbiased trajectory sampling.

Conformational dynamics that enable opening of the lipid translocation pathway are suppressed in the presence of cholesterol

Comparison of the tICA landscapes for the two sets of simulations (Figures 2C and 2G) reveals that the conformational sampling of the protein is much more limited in cholesterol-containing membranes, as a large part of the tICA space (defined by tIC1>5 and tIC2<−3) is not explored in the presence of cholesterol. To identify structural and kinetic characteristics of this unsampled region, we first discretized the tICA space in Figure 2C into 50 microstates and built an MSM to describe conformational transitions between these states (see STAR Methods). Then, the microstates were further grouped into 10 macrostates according to their kinetic similarity using PCCA+ analysis, and structural features of each macrostate were investigated. In particular, we monitored several variables shown in Figure 1 that were previously identified in Morra et al. (2018) to represent structural hallmarks of the lipid pathway opening. Thus, we calculated the minimal distance between residues E249$^{6.32}$ on TM6 and K311$^{7.58}$ on TM7 (d_{S1}) describing widening of the intracellular (IC) entrance to the lipid pathway (S1 site), and the minimal distance between residues C264$^{6.47}$ from TM6 and S298$^{7.45}$ from

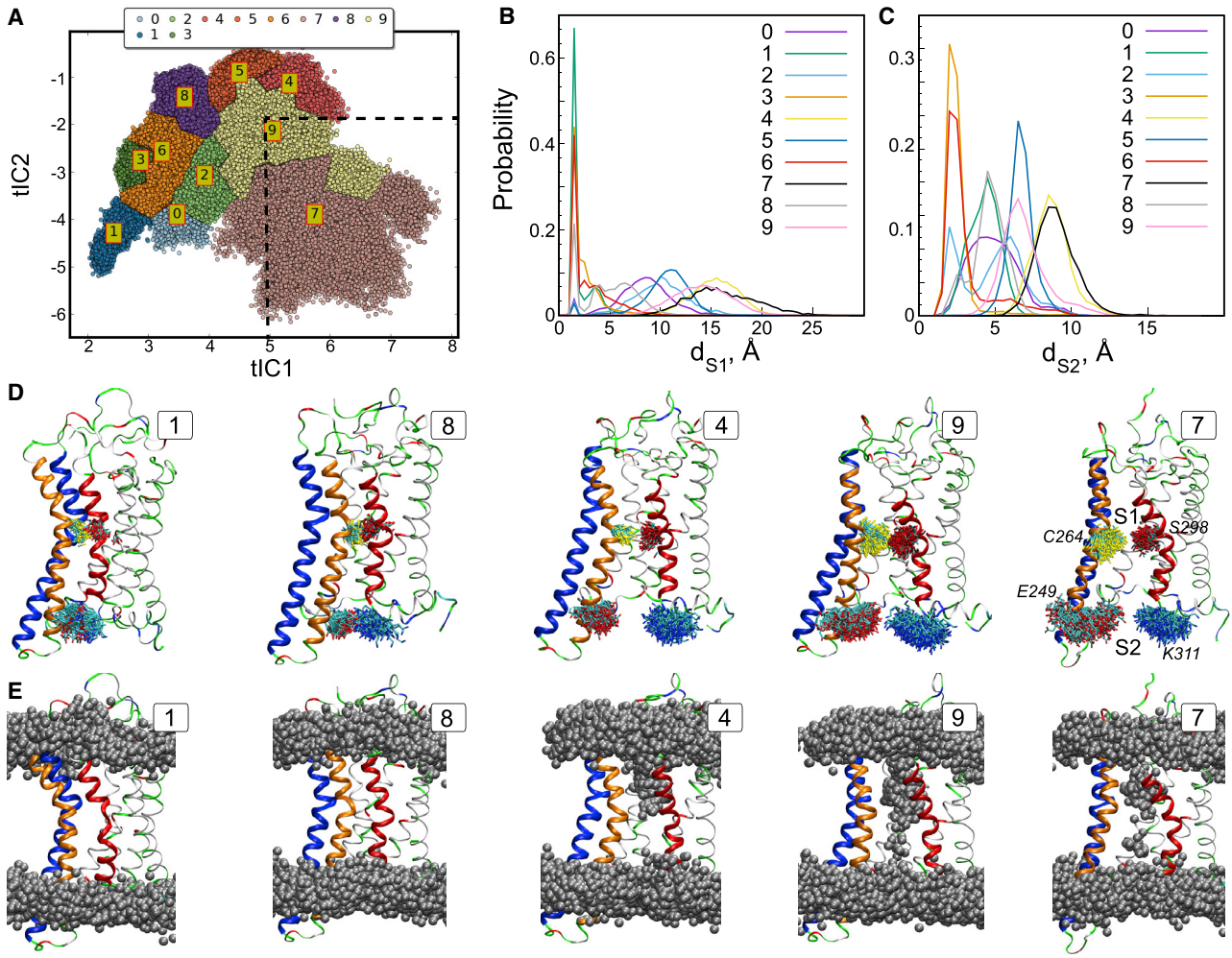

Figure 3. Structural analysis of macrostates on the tICA space built from 150-μs-long ensemble MD simulations of –Chol system

(A) Location of the 10 macrsotates on the 2D tICA space. The dashed lines mark the region (tIC1 > 5 and tIC2 < −2) unsampled in the simulations of the +Chol system.

(B and C) Histograms of d_{S1} (C) and d_{S2} (D) distances in each macrostate.

(D) Snapshots of the protein from selected macrostates (1, 4, 7, 8, and 9) showing different configurations of the S1 and S2 sites. Conformational sampling of residues E249$^{6.32}$, K311$^{7.58}$, C264$^{6.47}$, and S298$^{7.45}$ in each of these macrostates is shown by superposition of sidechain atoms of these residues in the trajectory frames from each macrostate. TMs 5, 6, and 7 are colored in blue, orange, and red.

(E) Snapshots of the protein and the lipid phosphorus (P) atoms (silver spheres) from selected macrostates (1, 4, 7, 8, and 9) illustrating various degrees of lipid penetration into the pathway. Shown are superpositions of P atoms in the trajectories from each macrostate.

TM7 (d_{S2}) describing opening of the middle region of the translocation pathway (S2 site). In addition, we monitored the extent of lipid penetration into the translocation pathway.

Figure 3A depicts locations of the 10 macrostates on the tICA space with Figures 3B and 3C showing distributions of d_{S1} and d_{S2} distances, respectively, in the trajectory frames from each macrostate. The results reveal that macrostates 4, 5, 7, and 9 largely contain protein conformations with both S1 and S2 sites in the open configuration (large d_{S1} and d_{S2}; see also visual representations in Figure 3D), consistent with an open lipid translocation pathway. Indeed, we find lipid headgroups populating the pathway in the trajectory frames from these macrostates (Figure 3E), with macrostates 7 and 9 specifically representing conformations in which the pathway is fully traversed by the lipid headgroups. Macrostate 4 combines conformations in which the translocation pathway is penetrated by the lipid tails, rather than their headgroups (data not shown). As described in our previous papers (Khelashvili et al., 2019; Morra et al., 2018), such modes of protein-lipid interaction decrease the overall hydration in the region, thus creating scrambling-incompetent conditions.

In the remaining macrostates (0, 1, 2, 3, 6, and 8), no lipid head group penetration is observed (Figure 3E), and the S2 site remains relatively closed. However, the configuration of the S1 site varies between these macrostates. Thus, the d_{S1} distance parameter has a pronounced peak at ∼2Å in microstate 1 (i.e., closed S1 site) but samples a progressively wider range along macrostates 3, 6, and 8. The opening of the S1 site continues in macrostates 0 and 2.

Consistent with the findings of Morra et al. (2018), our MSM analysis shows that the slowest kinetic processes in the system

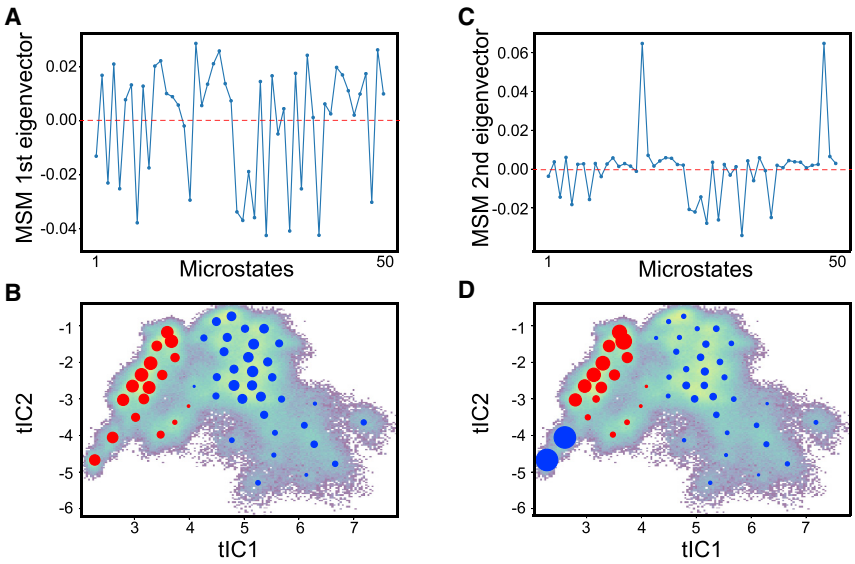

Figure 4. MSM analysis of lipid translocation process

(A and C) Contributions of the first two MSM eigenvectors (relaxation modes) to each microstate on the tICA space. The population exchanges between microstates with positive and negative eigenvectors.

(B and D) Representation of the first two MSM relaxation modes from (A) and (C) on the 2D tICA space. Red and blue circles show the location of the microstates with positive and negative contributions, respectively, to the relaxation modes. Microstates with larger circles contribute more to the relaxation mode (i.e., correspond to higher absolute value of the MSM eigenvector component).

correspond to transitions between states with closed S2 and S1 sites and those where the corresponding sites are open (Figures 4A and 4B, 1st MSM relaxation mode, ~37-μs timescales, and Figures 4C and 4D, 2nd MSM relaxation mode, ~24-μs timescales). Importantly, the structural analysis in Figure 3 reveals that the tICA space region that is unsampled in the cholesterol-rich membranes predominantly contains the ensemble of structures with a fully open lipid translocation pathway (in Figure 3A, see the region demarcated by the dashed lines). To gain a mechanistic understanding into how cholesterol may inhibit the opening of the lipid pathway, we studied the dynamics of cholesterol molecules around the protein.

We first investigated the relationship between the d_{S1} and d_{S2} distances and the level of lipid head group occupancy of the translocation pathway in the individual trajectories in cholesterol-free and cholesterol-rich membranes. Figure 5A shows d_{S1} versus d_{S2} in the 50 individual structures that were used as the starting points for the unbiased MD simulations, and Figure 5B shows the average values of these variables during each of the 3-μs-long MD simulations. As can be seen, a strong linear correlation between d_{S1} and d_{S2} is developed in the cholesterol-free systems (Pearson correlation coefficient R value = 0.8), whereas no such relationship was observed in the simulations containing cholesterol. Consistent with the overall trends inferred from the tICA/MSM analysis, we find that the simulations in which d_{S1} and d_{S2} sampled longer distances were also characterized with a larger extent of lipid head group penetration into the pathway. This is demonstrated in the d_{S1} versus d_{S2} plots in Figures 5C and 5D in which the datapoints from each simulation are colored according to the fraction of trajectory frames with at least one lipid head group found in the pathway (see also STAR Methods). As can be seen, the simulations in which $d_{S1} > 15$Å and $d_{S2} > 8$Å also show the strongest lipid penetration. These two distances remain relatively short in the cholesterol-rich membranes, and accordingly there is only a low level of lipid partitioning into the pathway in the corresponding simulations.

Cholesterol molecules engage with S2 site residues, thus inhibiting the opening of this region of the translocation pathway

We hypothesized that the reason why lipids were not seen near the S2 site in the simulations of cholesterol-rich membranes was because of a specific arrangement of cholesterol molecules at the TM6/7 interface that could block lipid access to the S2 site. To test this hypothesis, we investigated if cholesterol molecules populate the pathway and what is the mode of their interactions with the residues at S1 and S2 sites.

To this end, we aligned the trajectories so that the bilayer midplane z coordinate was at the origin (z = 0), and then we counted the number of cholesterol hydroxyl oxygen (O) atoms and phospholipid phosphorus (P) atoms within 3 Å of the protein and within a rectangle defined by $x \in [-5\text{Å}; 5\text{Å}]$, $y > 0$, and $z \in [-12\text{Å}; 12\text{Å}]$ (see Figure S2). Given the bilayer thickness of ~40 Å, this z range was chosen to capture events of the O and P atom penetration deep into the hydrophobic core of the bilayer in the protein vicinity, i.e., near the S2 site. As shown in Figures 6A and 6B, whereas the P atom density is relatively high in multiple trajectories in the cholesterol-depleted membranes, it is practically zero in the cholesterol-enriched membranes (compare cyan-colored symbols in Figures 6A and 6B). Instead, in these latter systems, we observe a large extent of cholesterol O atom penetration (lipid head group density is detected in only one trajectory).

Monitoring the time-evolution of cholesterol O atoms in the individual trajectories (Figure 6C) revealed several instances in which cholesterol molecules from either the IC or the EC leaflet partitioned into the middle of the bilayer in the vicinity of the S2 site. Indeed, such dynamics were observed in 19/50 trajectories (Figure S3), with residence times of the O atom near the S2 site ranging from a few nanoseconds to hundreds of nanoseconds (Figure 6D). In most cases, after excursion to the bilayer midplane area, cholesterol returned to the original leaflet. However, in five cases, cholesterol molecules underwent a complete flip between the leaflets (see the trajectories labeled with star symbol in Figure S3). Remarkably, in all five cases (irrespective of the scrambling direction), we found that during the flipping process, cholesterol transited through the S2 site with its polar hydroxyl group engaging primarily

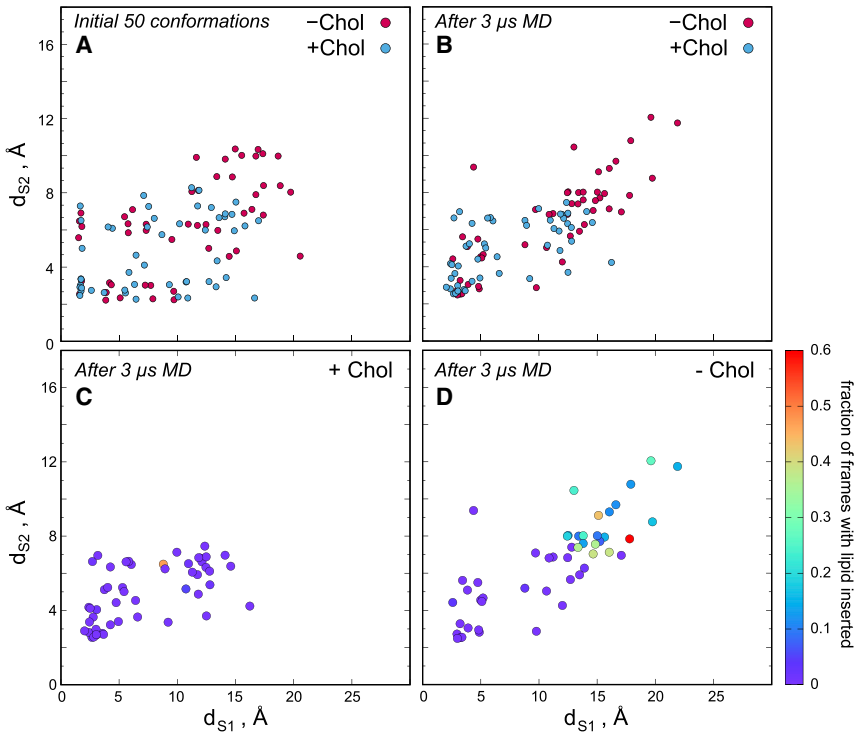

Figure 5. Cholesterol inhibits opening of the TM6/TM7 phospholipid translocation pathway

(A) d_{S1} versus d_{S2} in the 50 conformations used to initiate ensemble MD simulations of opsin in POPC/POPG (–Chol) and POPC/POPG/Cholesterol (+Chol) membranes.

(B) Average values of d_{S1} versus average values of d_{S2} in the 50 individual 3-μs simulations of opsin in POPC/POPG (–Chol) and POPC/POPG/Cholesterol (+Chol) membranes.

(C and D) The data from (B) are replotted separately for +Chol (C) and –Chol (D) systems by coloring each datapoint according to fraction of frames with at least one lipid head group inserted in the translocation pathway.

with S298$^{7.45}$ (see Figure 6D). However, the cholesterol translocation pathway did not go through the open hydrophilic conduit between TM6 and TM7 helices as observed for lipid scrambling. Rather, cholesterol appeared to associate strictly with the TM7 residues at the S2 site level while remaining largely in the bilayer (see state 2 in Figure 6D). Cholesterol flipping along the surface of a transmembrane protein has been reported previously from MD simulations (e.g., see Thangapandian et al. (2020) for cholesterol translocation associated with P-glycoprotein).

To obtain a more detailed characterization of specific modes of association between cholesterol and S2 site residues, we carried out a clustering analysis of the trajectory frames in which cholesterol was found at the S2 site. To this end, we first collected from each of the 19 trajectories described in Figures 6 and S3 all the snapshots displaying cholesterol in the vicinity of the S2 site. After aligning the resulting meta-trajectory, opsin-cholesterol complexes were clustered according to the position of the cholesterol hydroxyl group. The first five clusters covered 70% of the dataset and highlighted the cholesterol OH group coordinated by the oxygens of either T297$^{7.44}$ or S298$^{7.45}$ (as an example, Figure 7 shows structural representations of clusters 1–4). The body of the cholesterol molecule remained in the bilayer either adopting a transverse position, parallel to the bilayer plane (as in clusters 2 and 4), or assuming more tilted orientations (as in clusters 1 and 3). Thus, cholesterol partitioning at the S2 site is enabled by interactions with the polar residues on TM7; in contrast, S2 site residues on TM6 do not engage cholesterol. This mode of association keeps the sterol molecule largely away from the lipid translocation pathway as it flips between the leaflets, and in this process the S2 site remains relatively closed. Taken together with the results presented in Figures 6A and 6B, our data suggest that cholesterol molecules compete with phospholipids for the S2 site as they diffuse between the leaflets, thus inhibiting phospholipid scrambling.

DISCUSSION

The plasma membrane of mammalian cells has a large complement of different class A GPCRs yet exhibits no constitutive scramblase activity (Khelashvili and Menon, 2021; Kobayashi and Menon, 2018), a feature that enables signaling lipids such as phosphatidylserine to be ensconced in the inner leaflet until their surface exposure is triggered by physiological prompts that activate regulated scramblases such as TMEM16F (Nagata et al., 2020). We hypothesized that the unique physical properties of the plasma membrane, notably its high cholesterol content, may impact GPCR-mediated lipid scrambling in this membrane. As noted above (see introduction), the scramblase activity of GPCRs is more likely to be relevant in the early secretory pathway where membranes are cholesterol poor (Holthuis and Menon, 2014; Menon, 2018).

The influence of cholesterol on canonical GPCR activity is well established (Kiriakidi et al., 2019; Pucadyil and Chattopadhyay, 2006; Albert et al., 2016; Boesze-Battaglia and Albert, 1990; Guixa-Gonzalez et al., 2017; Huang et al., 2022; McGraw et al., 2019). While numerous studies have been devoted to understanding how cholesterol affects GPCR conformational dynamics as they pertain to cell signaling (e.g., see Kiriakidi et al., 2019; Guixa-Gonzalez et al., 2017; McGraw et al., 2019; Gimpl, 2016; Duncan et al., 2020; Sarkar et al., 2020 and citations therein), the effect of cholesterol on the scrambling dynamics of GPCRs has thus far not been explored. Therefore, it has remained unclear whether cholesterol can inhibit GPCR-mediated lipid scrambling, and if so, what mechanism might be at play.

There are potentially two, non-mutually exclusive mechanisms by which cholesterol may affect GPCR scrambling: (1) protein conformational dynamics necessary for scrambling activity are suppressed in a cholesterol-rich membrane because of the known general ordering effect of cholesterol on lipid bilayer properties (Regen, 2022), and (2) cholesterol competes with

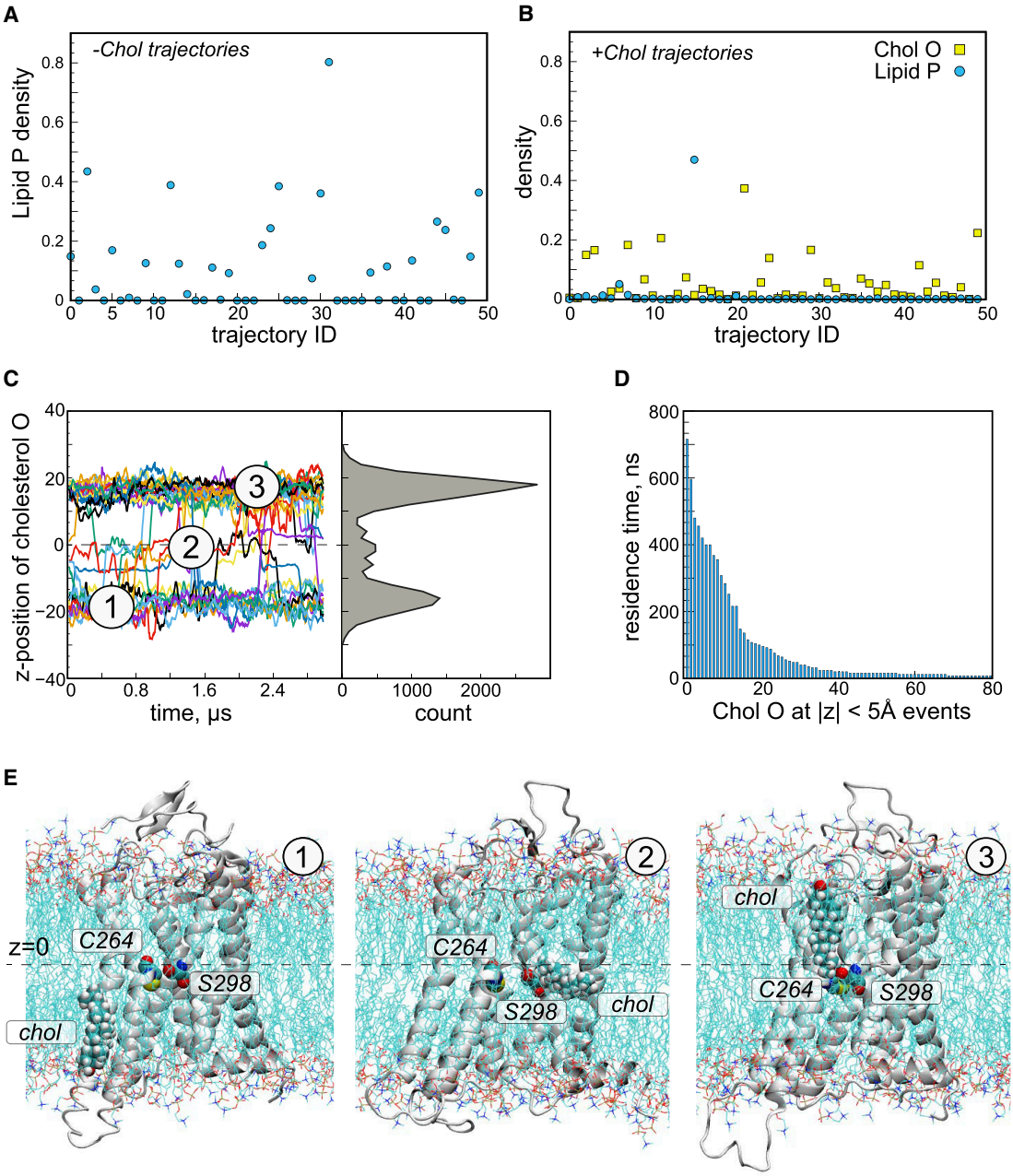

Figure 6. Cholesterol is scrambled via the TM6/TM7 pathway

(A) Fraction of trajectory frames with at least one lipid P atom within 3 Å of protein and within $z \in [-12Å; 12Å]$ in the set of opsin simulations in POPG/POPG membranes. z = 0 represents the bilayer midplane.

(B) Fraction of trajectory frames with at least one lipid P atom (cyan) or cholesterol O atom (yellow) within 3 Å of protein and within $z \in [-12Å; 12Å]$ in the set of opsin simulations in POPC/POPG/cholesterol membranes. z = 0 represents the bilayer midplane.

(C) Left panel shows time-evolution of the z position of the O atom of cholesterol molecules in the simulations of opsin in POPC/POPG/cholesterol membranes. Shown are traces for only those O atoms for which z position was 0 at least once in the trajectory, i.e., cholesterol molecule visited the bilayer midplane. States 1, 2, and 3 denote z positions where cholesterol is on the intracellular leaflet, in the middle of the membrane, and on the extracellular leaflet, respectively. Right panel shows the summarizing count histogram of z positions of cholesterol O atoms.

(D) Residence times for events of finding cholesterol O atom within $z \in [-5Å; 5Å]$ interval.

(E) Representative snapshots of opsin in POPC/POPG/cholesterol membrane corresponding to the z positional states 1, 2, and 3 marked in (C). In these snapshots, cholesterol molecule flips from the intracellular (state 1) to the extracellular (state 3) leaflet via intermediate conformation (state 2) where it interacts with its oxygen with S298$^{7.45}$ residues.

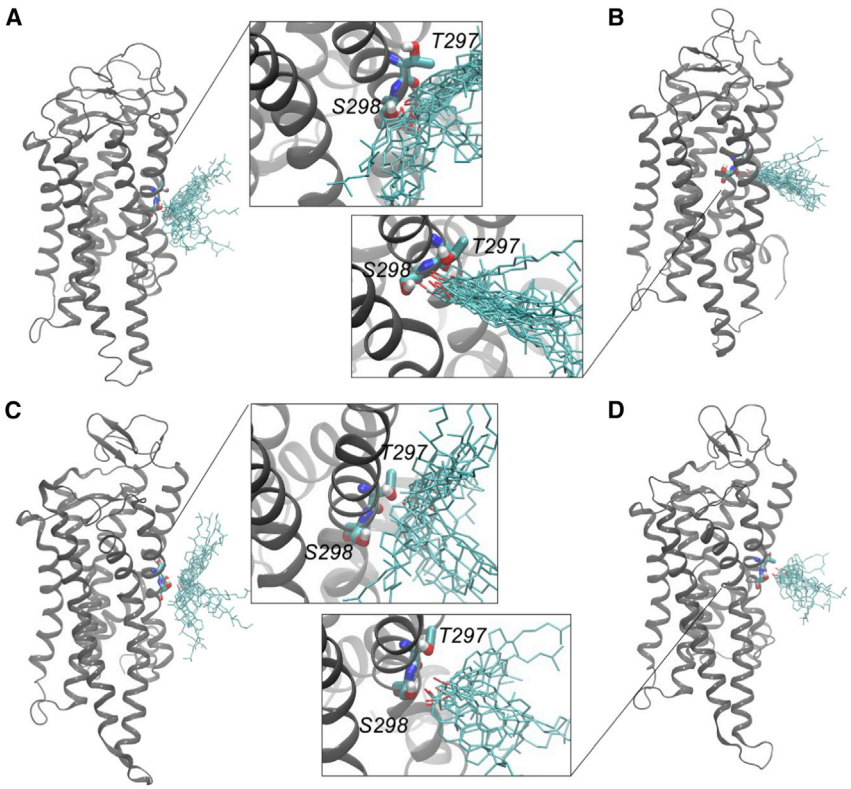

Figure 7. Modes of cholesterol arrangement at the S2 site of the translocation pathway

Clustering analysis of the O-H group of cholesterol molecules transiently binding to the S2 site in POPC/POPG/cholesterol membranes.

(A–D) show clusters 1, 2, 3, and 4, respectively. Zoom-in details are provided for each cluster showing the ensemble of conformations for the cholesterol molecules and a representative protein structure highlighting the positioning of residues S298$^{7.45}$ and T297$^{7.44}$ on TM7.

lipids for the translocation pathway and blocks them from entering the pathway.

The large-scale computational studies presented here build on our previous mechanistic investigation of opsin-mediated lipid scrambling (Morra et al., 2018) and present a comparative analysis of scrambling mechanisms in cholesterol-free versus cholesterol-rich membranes. The results reveal that in a cholesterol-rich membrane, the TM6/7 lipid translocation pathway is highly populated by cholesterol molecules while lipids are excluded from the pathway. Interestingly, in the absence of translocating phospholipids, the central region of the TM6/7 interface, the S2 site (see Figure 1), is predominantly found in a closed conformation. Cholesterol molecules, due to their small hydrophilic head group size, can still traverse the pathway via the S2 site and flip without the need for this part of the pathway to open. Thus, cholesterol molecules outcompete phospholipids for the pathway (Figure 8).

Whereas the competition aspect of the cholesterol effect would be expected to be statistical in nature, i.e., related to the cholesterol/phospholipid ratio, the mechanism is likely to

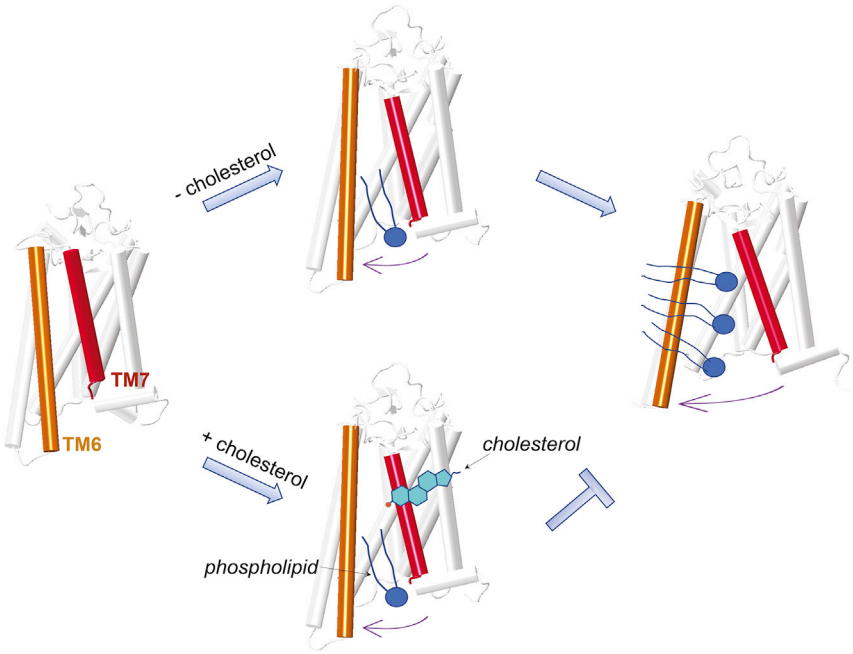

Figure 8. Schematic representation of the blocking mechanism of opsin-mediated lipid scrambling by cholesterol

TM6 and TM7 helices of opsin are shown in orange and red, respectively. Phospholipids and cholesterol are drawn as cartoons, with the O-H group of the cholesterol molecule highlighted as red circle (see text for more details).

be more complex. For example, it is unclear whether there is a minimal cholesterol concentration or threshold at which the observed blockage of the pathway can occur. Indeed, the inhibitory effect of cholesterol on lipid scrambling could be gradual, i.e., the blockage may occur already at relatively low cholesterol concentrations, and therefore, with increasing cholesterol content, a progressively larger number of opsin molecules would exhibit the blocked lipid translocation pathway. Alternatively, the inhibitory effect could take effect at some specific cholesterol concentration, so that the pathway remains accessible to lipids up to some threshold cholesterol concentration but becomes blocked once this threshold is exceeded. These two scenarios could, in principle, be distinguished by studying opsin-mediated lipid scrambling with *in vitro* reconstitution assays (Menon et al., 2011) using vesicles of various cholesterol compositions. These experimental tests will be critical in the future to validate our computational predictions.

STAR★METHODS

Detailed methods are provided in the online version of this paper and include the following:

- KEY RESOURCES TABLE
- RESOURCE AVAILABILITY
  - Lead contact
  - Materials availability
  - Data and code availability
- METHOD DETAILS
  - Molecular constructs for atomistic molecular dynamics (MD) simulations
  - MD simulation protocols
  - Dimensionality reduction with tICA approach
  - Markov State Model (MSM) construction
  - Clustering analysis of cholesterol positions around S2 site

SUPPLEMENTAL INFORMATION

Supplemental information can be found online at https://doi.org/10.1016/j.str.2022.05.010.

ACKNOWLEDGMENTS

This work was supported by National Institutes of Health grants R01 EY027969 and R21 EY028314 (to A.K.M. and G.K.). G.K. is also supported by the HRH Prince Alwaleed Bin Talal Bin Abdulaziz Alsaud Institute of Computational Biomedicine at Weill Cornell Medical College through a gratefully acknowledged support from the 1923 Fund. The authors gratefully acknowledge the use of resources of the Oak Ridge Leadership Computing Facility, which is a DOE Office of Science User Facility supported under Contract DE-AC05-00OR22725, and of in-house computational resources of the David A. Cofrin Center for Biomedical Information in the Institute for Computational Biomedicine at Weill Cornell Medical College.

AUTHOR CONTRIBUTIONS

G.K. and A.K.M. conceived the project. G.K. designed the study. G.M. performed the majority of the analyses. A.M.R. performed MD simulations and carried out Markov State Model analysis. All authors contributed to the interpretation of the data and writing the manuscript.

DECLARATION OF INTERESTS

The authors declare no competing interests.

Received: March 8, 2022
Revised: April 28, 2022
Accepted: May 11, 2022
Published: June 3, 2022

REFERENCES

Albert, A., Alexander, D., and Boesze-Battaglia, K. (2016). Cholesterol in the rod outer segment: a complex role in a "simple" system. Chem. Phys. Lipids *199*, 94–105. https://doi.org/10.1016/j.chemphyslip.2016.04.008.

Albert, A.D., and Boesze-Battaglia, K. (2005). The role of cholesterol in rod outer segment membranes. Prog. Lipid Res. *44*, 99–124. https://doi.org/10.1016/j.plipres.2005.02.001.

Ballesteros, J.A., and Weinstein, H. (1995). [19] Integrated methods for the construction of three-dimensional models and computational probing of structure-function relations in G protein-coupled receptors. Methods Neurosci. *40*, 366–428. https://doi.org/10.1016/s1043-9471(05)80049-7.

Beauchamp, K.A., Bowman, G.R., Lane, T.J., Maibaum, L., Haque, I.S., and Pande, V.S. (2011). MSMBuilder2: modeling conformational dynamics on the picosecond to millisecond scale. J. Chem. Theory Comput. *7*, 3412–3419. https://doi.org/10.1021/ct200463m.

Boesze-Battaglia, K., and Albert, A.D. (1990). Cholesterol modulation of photoreceptor function in bovine retinal rod outer segments. J. Biol. Chem. *265*, 20727–20730. https://doi.org/10.1016/s0021-9258(17)45275-6.

Chauhan, N., Farine, L., Pandey, K., Menon, A.K., and Butikofer, P. (2016). Lipid topogenesis–35years on. Biochim. Biophys. Acta *1861*, 757–766. https://doi.org/10.1016/j.bbalip.2016.02.025.

Daura, X., Gademann, K., Jaun, B., Seebach, D., van Gunsteren, W.F., and Mark, A.E. (1999). Peptide folding: when simulation meets experiment. Angew. Chem. Int. Ed. *38*, 236–240. https://doi.org/10.1002/(sici)1521-3773(19990115)38:1/2<236::aid-anie236>3.0.co;2-m.

Deuflhard, P., and Weber, M. (2005). Robust Perron cluster analysis in conformation dynamics. Linear Algebra Appl. *398*, 161–184. https://doi.org/10.1016/j.laa.2004.10.026.

Duncan, A.L., Song, W., and Sansom, M.S.P. (2020). Lipid-dependent regulation of ion channels and G protein-coupled receptors: insights from structures and simulations. Annu. Rev. Pharmacol. Toxicol. *60*, 31–50. https://doi.org/10.1146/annurev-pharmtox-010919-023411.

Eastman, P., Swails, J., Chodera, J.D., McGibbon, R.T., Zhao, Y., Beauchamp, K.A., Wang, L.P., Simmonett, A.C., Harrigan, M.P., Stern, C.D., et al. (2017). OpenMM 7: rapid development of high performance algorithms for molecular dynamics. PLoS Comput. Biol. *13*, e1005659. https://doi.org/10.1371/journal.pcbi.1005659.

Ernst, O.P., and Menon, A.K. (2015). Phospholipid scrambling by rhodopsin. Photochem. Photobiol. Sci. *14*, 1922–1931. https://doi.org/10.1039/c5pp00195a.

Essmann, U., Perera, L., Berkowitz, M.L., Darden, T., Lee, H., and Pedersen, L.G. (1995). A smooth particle mesh Ewald method. J. Chem. Phys. *103*, 8577–8593. https://doi.org/10.1063/1.470117.

Gimpl, G. (2016). Interaction of G protein coupled receptors and cholesterol. Chem. Phys. Lipids *199*, 61–73. https://doi.org/10.1016/j.chemphyslip.2016.04.006.

Goren, M.A., Morizumi, T., Menon, I., Joseph, J.S., Dittman, J.S., Cherezov, V., Stevens, R.C., Ernst, O.P., and Menon, A.K. (2014). Constitutive phospholipid scramblase activity of a G protein-coupled receptor. Nat. Commun. *5*, 5115. https://doi.org/10.1038/ncomms6115.

Guixa-Gonzalez, R., Albasanz, J.L., Rodriguez-Espigares, I., Pastor, M., Sanz, F., Marti-Solano, M., Manna, M., Martinez-Seara, H., Hildebrand, P.W., Martin, M., and Selent, J. (2017). Membrane cholesterol access into a G-protein-coupled receptor. Nat. Commun. *8*, 14505. https://doi.org/10.1038/ncomms14505.

Harrigan, M.P., Sultan, M.M., Hernandez, C.X., Husic, B.E., Eastman, P., Schwantes, C.R., Beauchamp, K.A., McGibbon, R.T., and Pande, V.S.

(2017). MSMBuilder: statistical models for biomolecular dynamics. Biophys. J. *112*, 10–15. https://doi.org/10.1016/j.bpj.2016.10.042.

Holthuis, J.C., and Menon, A.K. (2014). Lipid landscapes and pipelines in membrane homeostasis. Nature *510*, 48–57. https://doi.org/10.1038/nature13474.

Huang, J., Rauscher, S., Nawrocki, G., Ran, T., Feig, M., de Groot, B.L., Grubmuller, H., and MacKerell, A.D., Jr. (2017). CHARMM36m: an improved force field for folded and intrinsically disordered proteins. Nat. Methods *14*, 71–73. https://doi.org/10.1038/nmeth.4067.

Huang, S.K., Almurad, O., Pejana, R.J., Morrison, Z.A., Pandey, A., Picard, L.P., Nitz, M., Sljoka, A., and Prosser, R.S. (2022). Allosteric modulation of the adenosine A2A receptor by cholesterol. Elife *11*, e73901. https://doi.org/10.7554/elife.73901.

Jo, S., Lim, J.B., Klauda, J.B., and Im, W. (2009). CHARMM-GUI membrane builder for mixed bilayers and its application to yeast membranes. Biophys. J. *97*, 50–58. https://doi.org/10.1016/j.bpj.2008.12.109.

Khelashvili, G., Falzone, M.E., Cheng, X., Lee, B.C., Accardi, A., and Weinstein, H. (2019). Dynamic modulation of the lipid translocation groove generates a conductive ion channel in Ca(2+)-bound nhTMEM16. Nat. Commun. *10*, 4972. https://doi.org/10.1038/s41467-019-12865-4.

Khelashvili, G., and Menon, A.K. (2021). Phospholipid scrambling by G protein-coupled receptors. Annu. Rev. Biophys. *51*, 39–61. https://doi.org/10.1146/annurev-biophys-090821-083030.

Kiriakidi, S., Kolocouris, A., Liapakis, G., Ikram, S., Durdagi, S., and Mavromoustakos, T. (2019). Effects of cholesterol on GPCR function: insights from computational and experimental studies. Adv. Exp. Med. Biol. *1135*, 89–103. https://doi.org/10.1007/978-3-030-14265-0_5.

Kobayashi, T., and Menon, A.K. (2018). Transbilayer lipid asymmetry. Curr. Biol. *28*, R386–R391. https://doi.org/10.1016/j.cub.2018.01.007.

Lee, B.C., Khelashvili, G., Falzone, M., Menon, A.K., Weinstein, H., and Accardi, A. (2018). Gating mechanism of the extracellular entry to the lipid pathway in a TMEM16 scramblase. Nat. Commun. *9*, 3251. https://doi.org/10.1038/s41467-018-05724-1.

McGraw, C., Yang, L., Levental, I., Lyman, E., and Robinson, A.S. (2019). Membrane cholesterol depletion reduces downstream signaling activity of the adenosine A2A receptor. Biochim. Biophys. Acta Biomembr. *1861*, 760–767. https://doi.org/10.1016/j.bbamem.2019.01.001.

Menon, A.K. (2018). Sterol gradients in cells. Curr. Opin. Cell Biol. *53*, 37–43. https://doi.org/10.1016/j.ceb.2018.04.012.

Menon, I., Huber, T., Sanyal, S., Banerjee, S., Barre, P., Canis, S., Warren, J.D., Hwa, J., Sakmar, T.P., and Menon, A.K. (2011). Opsin is a phospholipid flippase. Curr. Biol. *21*, 149–153. https://doi.org/10.1016/j.cub.2010.12.031.

Molday, R.S., Garces, F.A., Scortecci, J.F., and Molday, L.L. (2021). Structure and function of ABCA4 and its role in the visual cycle and Stargardt macular degeneration. Prog. Retin. Eye Res. 101036. https://doi.org/10.1016/j.preteyeres.2021.101036.

Molday, R.S., and Molday, L.L. (1987). Differences in the protein composition of bovine retinal rod outer segment disk and plasma membranes isolated by a ricin-gold-dextran density perturbation method. J. Cell Biol. *105*, 2589–2601. https://doi.org/10.1083/jcb.105.6.2589.

Morra, G., Razavi, A.M., Pandey, K., Weinstein, H., Menon, A.K., and Khelashvili, G. (2018). Mechanisms of lipid scrambling by the G protein-coupled receptor opsin. Structure *26*, 356–367.e3. https://doi.org/10.1016/j.str.2017.11.020.

Nagata, S., Sakuragi, T., and Segawa, K. (2020). Flippase and scramblase for phosphatidylserine exposure. Curr. Opin. Immunol. *62*, 31–38. https://doi.org/10.1016/j.coi.2019.11.009.

Olsson, M.H.M., Sondergaard, C.R., Rostkowski, M., and Jensen, J.H. (2011). PROPKA3: consistent treatment of internal and surface residues in Empirical pKa predictions. J. Chem. Theory Comput. *7*, 525–537. https://doi.org/10.1021/ct100578z.

Park, J.H., Morizumi, T., Li, Y., Hong, J.E., Pai, E.F., Hofmann, K.P., Choe, H.W., and Ernst, O.P. (2013). Opsin, a structural model for olfactory receptors? Angew Chem. Int. Ed. Engl. *125*, 11227–11230. https://doi.org/10.1002/ange.201302374.

Perez-Hernandez, G., Paul, F., Giorgino, T., De Fabritiis, G., and Noe, F. (2013). Identification of slow molecular order parameters for Markov model construction. J. Chem. Phys. *139*, 015102,. https://doi.org/10.1063/1.4811489.

Phillips, J.C., Braun, R., Wang, W., Gumbart, J., Tajkhorshid, E., Villa, E., Chipot, C., Skeel, R.D., Kale, L., and Schulten, K. (2005). Scalable molecular dynamics with NAMD. J. Comput. Chem. *26*, 1781–1802. https://doi.org/10.1002/jcc.20289.

Pomorski, T., and Menon, A.K. (2006). Lipid flippases and their biological functions. Cell. Mol. Life Sci. *63*, 2908–2921. https://doi.org/10.1007/s00018-006-6167-7.

Pucadyil, T.J., and Chattopadhyay, A. (2006). Role of cholesterol in the function and organization of G-protein coupled receptors. Prog. Lipid Res. *45*, 295–333. https://doi.org/10.1016/j.plipres.2006.02.002.

Quazi, F., Lenevich, S., and Molday, R.S. (2012). ABCA4 is an N-retinylidene-phosphatidylethanolamine and phosphatidylethanolamine importer. Nat. Commun. *3*, 925. https://doi.org/10.1038/ncomms1927.

Quazi, F., and Molday, R.S. (2014). ATP-binding cassette transporter ABCA4 and chemical isomerization protect photoreceptor cells from the toxic accumulation of excess 11-cis-retinal. Proc. Natl. Acad. Sci. U S A *111*, 5024–5029. https://doi.org/10.1073/pnas.1400780111.

Razavi, A.M., Khelashvili, G., and Weinstein, H. (2017). A Markov state-based quantitative kinetic model of sodium release from the dopamine transporter. Sci. Rep. *7*, 40076. https://doi.org/10.1038/srep40076.

Razavi, A.M., Khelashvili, G., and Weinstein, H. (2018). How structural elements evolving from bacterial to human SLC6 transporters enabled new functional properties. BMC Biol. *16*, 31. https://doi.org/10.1186/s12915-018-0495-6.

Regen, S.L. (2022). Cholesterol's condensing effect: unpacking a century-old mystery. JACS Au *2*, 84–91. https://doi.org/10.1021/jacsau.1c00493.

Ruggiero, L., Connor, M.P., Chen, J., Langen, R., and Finnemann, S.C. (2012). Diurnal, localized exposure of phosphatidylserine by rod outer segment tips in wild-type but not Itgb5-/- or Mfge8-/- mouse retina. Proc. Natl. Acad. Sci. U S A *109*, 8145–8148. https://doi.org/10.1073/pnas.1121101109.

Sarkar, P., Mozumder, S., Bej, A., Mukherjee, S., Sengupta, J., and Chattopadhyay, A. (2020). Structure, dynamics and lipid interactions of serotonin receptors: excitements and challenges. Biophys. Rev. *13*, 101–122. https://doi.org/10.1007/s12551-020-00772-8.

Taghon, G.J., Rowe, J.B., Kapolka, N.J., and Isom, D.G. (2021). Predictable cholesterol binding sites in GPCRs lack consensus motifs. Structure *29*, 499–506.e3. https://doi.org/10.1016/j.str.2021.01.004.

Thangapandian, S., Kapoor, K., and Tajkhorshid, E. (2020). Probing cholesterol binding and translocation in P-glycoprotein. Biochim. Biophys. Acta Biomembr. *1862*, 183090. https://doi.org/10.1016/j.bbamem.2019.183090.

Van der Spoel, D., Lindahl, E., Hess, B., Groenhof, G., Mark, A.E., and Berendsen, H.J.C. (2005). GROMACS: fast, flexible, and free. J. Comput. Chem. *26*, 1701–1718. https://doi.org/10.1002/jcc.20291.

Venable, R.M., Luo, Y., Gawrisch, K., Roux, B., and Pastor, R.W. (2013). Simulations of anionic lipid membranes: development of interaction-specific ion parameters and validation using NMR data. J. Phys. Chem. B *117*, 10183–10192. https://doi.org/10.1021/jp401512z.

STAR★METHODS

KEY RESOURCES TABLE

REAGENT or RESOURCE	SOURCE	IDENTIFIER
Software and algorithms		
NAMD 2.10	Dr. Klaus Schulten (free software and publically available)	http://www.ks.uiuc.edu/Research/namd/
VMD	Dr. Klaus Schulten (free software and publically available)	http://www.ks.uiuc.edu/Research/vmd/
CHARMM-GUI	Dr. Wonpil Im (free web-based interface and publically available)	http://charmm-gui.org/
OpenMM 7.4	Dr. Gianni de Fabritiis Dr. John Chodera (molecular dynamics software for GPUs)	https://openmm.org
MSMBuilder	Dr. Vijay S Pande (software tool for building Markov State Models)	http://msmbuilder.org/3.8.0/

RESOURCE AVAILABILITY

Lead contact

Further information and requests for resources and reagents should be directed to and will be fulfilled by the lead contact George Khelashvili (gek2009@med.cornell.edu).

Materials availability

This study did not generate new unique reagents.

Data and code availability

Requests for the structural models and MD simulation trajectories should be directed to and will be fulfilled by the Lead contact.
This paper does not report original code.
Any additional information required to reanalyze the data reported in this paper is available from the Lead contact upon request.

METHOD DETAILS

Molecular constructs for atomistic molecular dynamics (MD) simulations

All the computations described here were based on our previously published ensemble MD simulations of opsin in 9:1 (mole/mole) mixture of POPC (1-palmitoyl-2-oleoyl-*sn*-glycero-3-phosphocholine) and POPG (1-palmitoyl-2-oleoyl-*sn*-glycero-3-phospho-(1′-rac-glycerol)) lipids (mimicking the composition of the reconstituted vesicles that have been used for scrambling activity assays (Goren et al., 2014)), described in Morra et al. (Morra et al., 2018). In these simulations, the protein to lipid ratio was 1:330 and the opsin X-ray structure from PDB: 4J4Q (Park et al., 2013) was used (the synthetic GαCT peptide as well as all non-protein components also present in the X-ray structure were not included). The opsin model in this PDB structure comprises residues 1–326. All the protonation states were determined at pH 7 using PropKa software (Olsson et al., 2011) which predicted all the titratable residues in their natural state.

As described in Results, to initiate a new set of simulations of opsin in the same membrane, 50 structures from the previous trajectory set were selected and each was subjected to 3 μs MD simulations (i.e., total sampling time of 150 μs). To create a system with opsin in cholesterol-enriched membranes, we extracted the coordinates of the protein from 4 frames in the same previous trajectory set (see Results), and using CHARMM-GUI (Jo et al., 2009), embedded these 4 opsin protein conformations in a new membrane containing 60:30:10 mixture of POPC, cholesterol, and POPG (i.e., a cholesterol-enriched membrane mixture) using a protein to lipid ratio of 1:322. These opsin-membrane complexes were solvated with a box containing 150 mM K^+Cl^- to achieve the final system size of $\sim$110,000 atoms.

MD simulation protocols

Using NAMD version 2.10 (Phillips et al., 2005), the four cholesterol-containing systems were first subjected to the multi-stage equilibration protocol prescribed by CHARMM-GUI. After this phase, for each of the four constructs ensemble MD simulations

were initiated in 20 replicates, each ran for 800 ns (i.e., total sampling time of 64 μs). These simulations were carried out with OpenMM 7.4 software (Eastman et al., 2017) and implemented PME for electrostatic interactions (Essmann et al., 1995). The runs were performed at 310K temperature, under NPT ensemble using semi-isotropic pressure coupling, and with 4fs integration time-step (with mass repartitioning). Monte Carlo barostat and Langevin thermostat were used to maintain constant pressure and temperature, respectively, in the simulations. Additional parameters for these runs included: "friction" set to 1.0/picosecond, "EwaldErrorTolerance" 0.0005, "rigidwater" True, and "ConstraintTolerance" 0.000001. The van der Waals interactions were calculated applying a cutoff distance of 12 Å and switching the potential from 10 Å.

The resulting set of simulations were analyzed using a dimensionality reduction approach (see below and Results) to select 50 structures for subsequent 3 μs MD simulations on each of them (i.e., total sampling time for these new runs was 150 μs). This set of simulations, as well as the one performed on 50 replicates in cholesterol-depleted membrane, also used OpenMM 7.4 software and implemented the same set of run parameters described above. For all simulations we used the latest CHARMM36m force-field for proteins and lipids (Huang et al., 2017), as well as recently revised CHARMM36 force-field for ions (Venable et al., 2013).

Dimensionality reduction with tICA approach

To facilitate analysis of conformational dynamics in the simulations, we performed dimensionality reduction using tICA (time-lagged independent component analysis) approach (Perez-Hernandez et al., 2013) as previously described (Khelashvili et al., 2019; Lee et al., 2018; Morra et al., 2018; Razavi et al., 2017, 2018). Briefly, in tICA, MD simulation trajectories are used to construct two covariance matrices, time-lagged covariance matrix (TLCM): $C_{TL}(\tau)=\langle X(t)XT(t+\tau)\rangle$ and the usual covariance matrix $C=\langle X(t)XT(t)\rangle$, where $X(t)$ is the data vector at time t, τ is the lag-time of the TLCM, and the symbol $\langle\ldots\rangle$ denotes the time average. To identify the slowest reaction coordinates of the system, the following generalized eigenvalue problem is solved: $C_{TL}V = C\,V\Lambda$, where Λ and V are the eigenvalue and eigenvector matrices, respectively. The eigenvectors corresponding to the largest eigenvalues define the slowest reaction coordinates. These reaction coordinates depend on the choice of data vector X, i.e., the choice of collective variables (CV). As CVs, we used 203 pairwise minimum distances between the heavy atoms of residues on TM3-TM5, TM3-TM6, TM3-TM7, TM5-TM6, TM5-TM7, and TM6-TM7 helices, as well as between the residues on 311–318 stretch in H8 helical segment and TM3, TM5, and TM6 (see Figure S1A). Note that this set of CVs is different from the one used in the analysis of biased MD simulations in Morra et al. (Morra et al., 2018) where much larger set of 2016 parameters were used (pairwise distances between every third residues in all 7 TMs). We found that the smaller number of CVs selected here for analyzing the new unbiased ensemble simulations yielded satisfactory Markovian behavior when building kinetic models (see below) and therefore was used throughout. The analysis of contributions of each tIC eigenvector to the total conformational fluctuations revealed that the first 2 tICs contained ~60% of the total fluctuations of the system (Figure S1B) and were sufficient to capture the protein dynamics related to lipid scrambling (see Results). Therefore, they were used to represent the trajectory frames in a dimensionality reduced space, and for the construction of kinetic models as described in the next section.

Markov State Model (MSM) construction

We constructed MSMs from 150 μs long simulation trajectories of opsin in the cholesterol-depleted membrane to quantify kinetics of protein conformational transitions related to lipid scrambling events. To this end, we used MSMBuilder software (Beauchamp et al., 2011; Harrigan et al., 2017) and a procedure described in Ref (Razavi et al., 2017). Briefly, the 2D tICA space was discretized into 50 microstates using automated clustering *k-means* algorithm, and a transition probability matrix (TPM) was built (Beauchamp et al., 2011). To ensure Markovian behavior, multiple TPMs were constructed for different time intervals between transitions (MSM lag times), and the relaxation timescales of the system were calculated as:

$$\tau_i = \frac{\tau'}{\ln \lambda_i}$$

where τ' is the lag-time used for building the TPM, λ_i denotes the i^{th} eigenvalue of the TPM, and τ_i represents relaxation timescale (implied timescale) corresponding to the i^{th} relaxation mode of the system. The Markovian property of the TPM was established by verifying the independence of τ_i from τ'. As shown in Figure S1C, the analysis identified 1.2 μs as the lag-time at which the implied timescales plots appear to converge. Thus, the final MSM was built using τ' = 1.2 μs.

To facilitate structural analysis of different regions on the 2D tICA space, using the TPM matrix, the microstate-level representation of the tICA space was transformed into a coarser description by lumping microstates together based on their kinetic similarity, and clustered into macrostates using the Robust Perron Cluster Analysis (PCCA+) (Deuflhard and Weber, 2005) algorithm.

Clustering analysis of cholesterol positions around S2 site

The presence of cholesterol in the vicinity of site S2 was investigated by counting how often in each trajectory an oxygen (O) atom from cholesterol was found in the volume delimited by the average positions of C_α atoms of C264 and S298 (Figure S2), with a tolerance of 3 Å, after trajectory alignment to the starting conformation. Every snapshot containing the O atom in the detection volume was collected into a meta-trajectory which contained frame-by-frame coordinates of only opsin and the cholesterol molecule found in the defined region. The GROMOS clustering approach (Daura et al., 1999) implemented in GROMACS (Van der Spoel et al., 2005), with a cutoff of 2 Å, was then applied to the meta-trajectory to generate clusters of the orientation of the cholesterol O-H segment.